Supplementary Information

Tuning La-O adsorption sites dispersion via hydrogen bond-capping organic-inorganic copolymerization strategy for enhanced phosphate removal

Feng Xiao[1], Yongqi Li[1], Shijie Wang[1], Jianing Zhang[1], Jia Hong Pan[2], Dongqin Yuan[3], Shuoxun Dong[1]* and Yili Wang[3]

1: School of Water Resources and Hydropower Engineering, North China Electric Power University, Beijing 102206, China

2: State Key Laboratory of Featured Metal Materials and Life-Cycle Safety for Composite Structures, School of Resources, Environment and Materials, Guangxi University, Nanning 530004, Guangxi, China

3: College of Environmental Science and Engineering, Beijing Key Lab for Source Control Technology of Water Pollution, Beijing Forestry University, Beijing 100083, China

Table of Contents

*Corresponding author. E-mail address: dongshuoxun@ncepu.edu.cn (S. Dong).

Section S1. Materials Preparation

Preparation of PVA-LHO copolymerized hydrogel (LaCPVA), pure PVA hydrogel and La-NP modified PVA hydrogel (La-PVA)

PvaLaC was prepared through the following repeated freezing-and-melting method. Initially, 10 mL of LHO at a concentration of 50 mg/mL was centrifuged at 8000 rpm for 5 min, and then the supernatant was removed. Aqueous solutions containing 10 wt. % PVA were formed by dissolving PVA in deionized water at 90°C for 6 h. The PVA aqueous solution was then uniformly mixed with the LHO precipitate to obtain a homogeneous emulsion. Next, the PVA solution was frozen using an ultra-low temperature upright freezer maintained at -74±2°C. After 12 h, the frozen sample was thawed at room temperature for 6 h. This freeze and melt cycle were repeated three times. The pure PVA hydrogel was synthesized using the same procedure as mentioned above without the use of LHO. La-PVA was synthesized by substituting LHO with a La-NP solution.

Preparation of PAM-LHO copolymerized hydrogel (LaCPAM), pure PAM hydrogel and La-NP modified PAM hydrogel (La-PAM)

Initially, 10 mL of the LHO solution (50 mg/mL) was centrifugated for 5 min at 8000 rpm, and the supernatant was discarded. Next, an aqueous AM solution (1.0 g of AM dissolved in 4 mL of H_2O) was mixed uniformly with the LHO precipitate to generate a homogeneous emulsion. Subsequently, 4 mL of an MBAA alcoholic solution (5 mg/L) was added to the emulsion under vigorous stirring. Finally, 0.4 mL of a saturated KPS ethanol solution and 20 μL of TEMED were added to the mixture, which

had been pre-deoxygenated with N_2 gas for 30 min. After a copolymerization reaction at 25°C for 24 h, the resulting white gel was washed with ethanol and deionized water to eliminate any residues, then dried under vacuum at -40°C for 24 h, resulting in the formation of bulk PamLaC. A pure PAM hydrogel was synthesized by following the procedure outlined above, excluding the inclusion of LHO. La-PAM was prepared by substituting LHO with a solution of La-NP.

Section S2. Adsorption Models

The isothermal adsorption curves were analyzed using the Langmuir and Freundlich equations. The Langmuir equation is formulated as follows:

$$q_e = \frac{q_m b C_e}{1 + b q_m}$$

where q_e represents the equilibrium adsorption concentration (mg/L), C_e is the equilibrium liquid-phase concentration (mg/L), q_m is the theoretical saturation sorption capacity (mg/g), b is a constant related to the adsorption heat [1]. The reliability of Langmuir equation could be assessed using the value of R_L as below:

$$R_L = \frac{1}{1 + b C_0}$$

where C_0 is the initial adsorbent concentration. When $0<R_L\leqslant 1$, the experiment data could fit the Langmuir model; when $R_L = 0$ or $R_L>1$, the experiment data could not fit the model.

The Freundlich equation was utilized to describe non-ideal and multi-layer adsorption on heterogeneous adsorbents' surfaces [2]. The Freundlich equation is expressed as:

$$q_e = K_F C_e^{1/n}$$

Alternatively, this equation can be linearized as:

$$\lg q_e = \frac{1}{n}\lg C_e + lgK_F$$

where K_F (mg^{1+n} L^n/g) and n are Freundlich constants.

The adsorption kinetics were performed in 100 mL of a 100.0 mg P/L solution at a dosage of 0.3 g/L at pH 7.0±0.2 agitated for 1.5 h at 300 rpm/min under 25°C. The pseudo-first-order (PFO) kinetic equation and pseudo-second-order (PSO) kinetic equation was applied to analyze adsorption kinetics.

The Liu isotherm model represents a synergistic amalgamation of the Langmuir and Freundlich isotherm models, with a departure from the Langmuir model's monolayer adsorption hypothesis and the Freundlich model's assumption of an unlimited adsorption capacity [3]. This approach posits that the active sites on the adsorbent surface exhibit a heterogeneous distribution of energies. The Liu equation is as follows:

$$q_e = \frac{Q_{max}(K_g C_e)}{1 + (K_g C_e)^{n_L}}$$

where K_g is the Liu equilibrium constant (L/mg); n_L is dimensionless exponent of the Liu equation, and Q_{max} is the maximum adsorption capacity of the adsorbent (mg/g).

The usage of La (g_{La}) was calculated as follows:

$$g_{La} = \frac{Q_{LaCCH} - Q_{CH}}{W_{La}}$$

where Q_{LaCCH} (mg/g) is the maximum adsorption capacity of LaCCH, Q_{CH} is the

adsorption capacity of CH at the same equilibrium adsorption concentration calculated by the isotherm model, W_{La} is La element content (wt%) in LaCCH.

The PFO rate expression based on capacity is generally expressed as follows:

$$\frac{dq_t}{dt} = k_1(q_e - q_t)$$

Where K_1 (min^{-1}) is the PFO rate constant; q_e (mg/g) and q_t (mg/g) are the amount of P adsorbed per unit weight of the adsorbent at equilibrium and time t.

The PSO equation is also based on the sorption capacity, which is expressed as follows:

$$\frac{dq_t}{dt} = k_2(q_e - q_t)^2$$

this equation also could be expressed by a linear model as follows:

$$\frac{t}{q_t} = \frac{1}{k_2 q_e^2} + \frac{1}{q_e}t$$

Where k_2 (g/(mg· min)) is the rate constant of second-order adsorption.

Section S2. Supplemental Figures and Tables

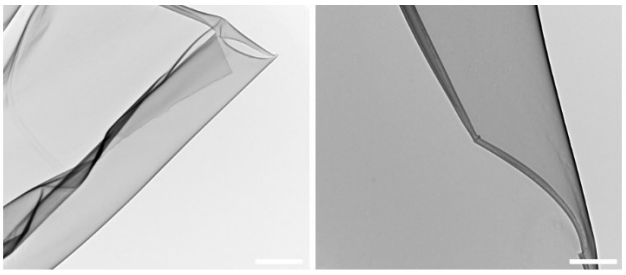

Fig. S1 Ultrathin slices TEM images of CH.

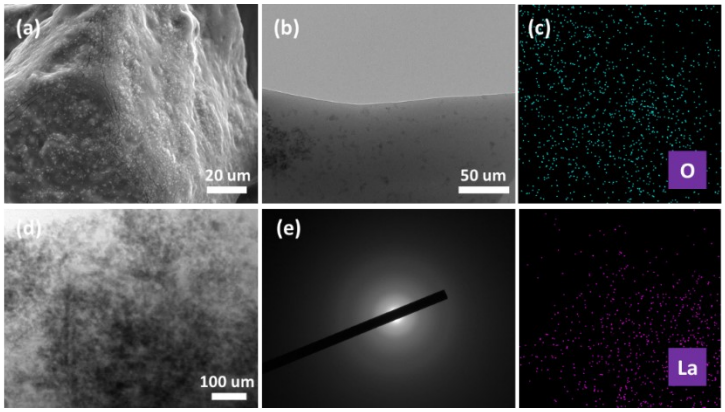

Fig. S2 SEM-EDS mapping (a-c), TEM (d) and SAED (e) images of LaCCH.

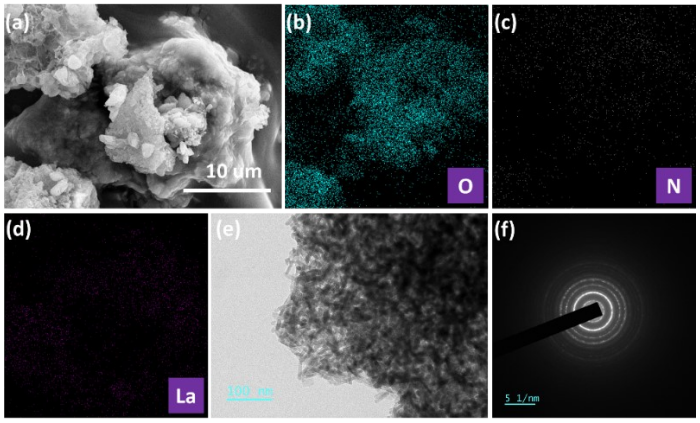

Fig. S3 SEM-EDS mapping (a-d), TEM (e) and SAED (f) images of La-CH.

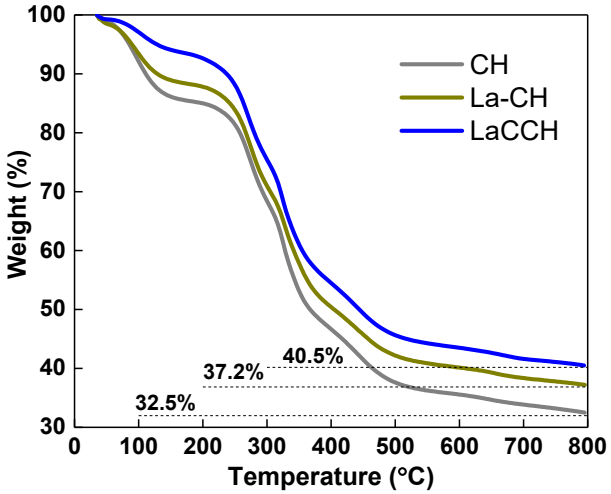

Fig. S4 TGA curves of LaCCH, La-CH and CH.

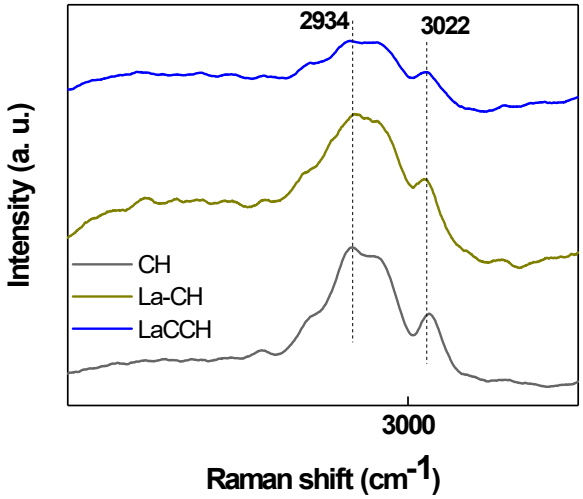

Fig. S5 Raman spectra of LaCCH, La-CH and CH.

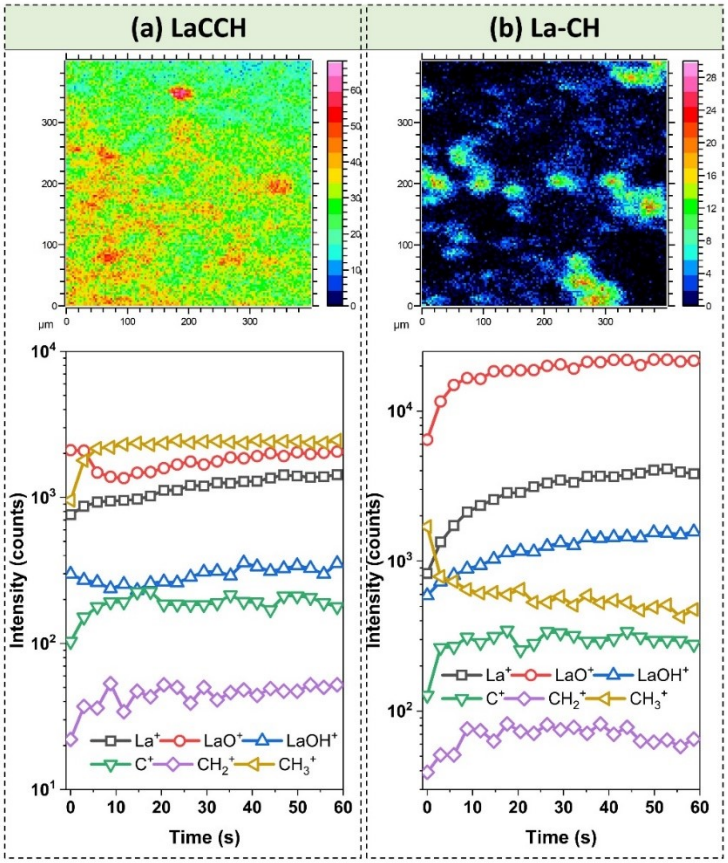

Fig. S6 Reconstructed 2D ToF-SIMS images of La^+ after 60 s sputtering, and Dynamic ToF-SIMS depth profiling of LaCCH (a) and La-CH (b). A darker color represents a stronger signal intensity.

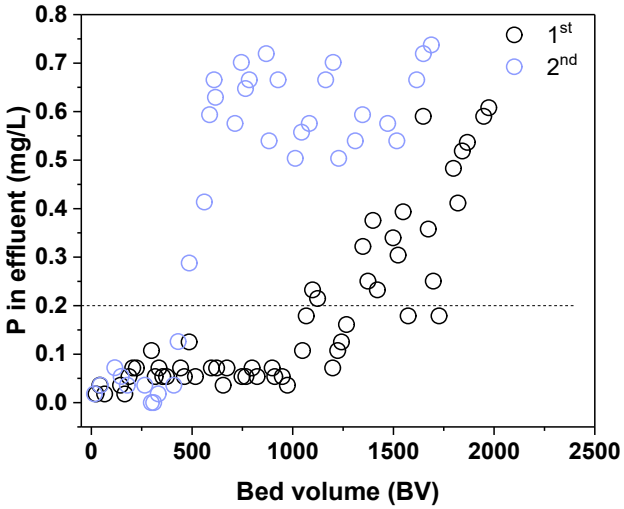

Fig. S7 Breakthrough curve of P adsorption by LaCCH with the feeding of a simulated effluent (TP=1.0 mg/L; COD=500 mg/L; [NaCl]=500 mg/L; [$NaNO_3$-N]=50 mg/L; [NH_4-N]=20 mg/L; pH=6.90-7.15; EBCT=6.25 BV/h, adsorbent dosage: 0.18 g/cm).

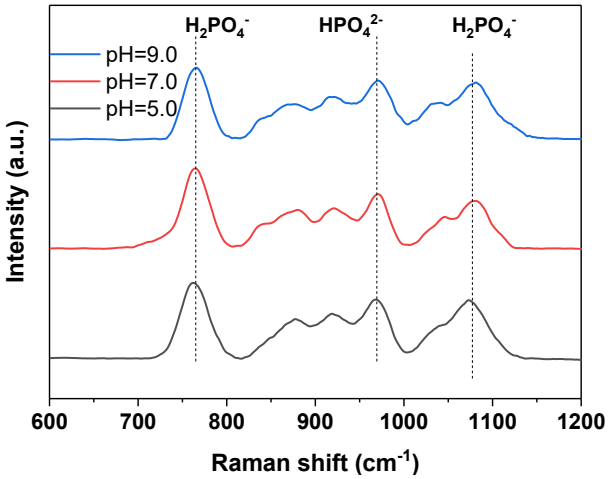

Fig. S8 Raman spectroscopy spectra of the LaCCH after P adsorption at pH=5.0-9.0.

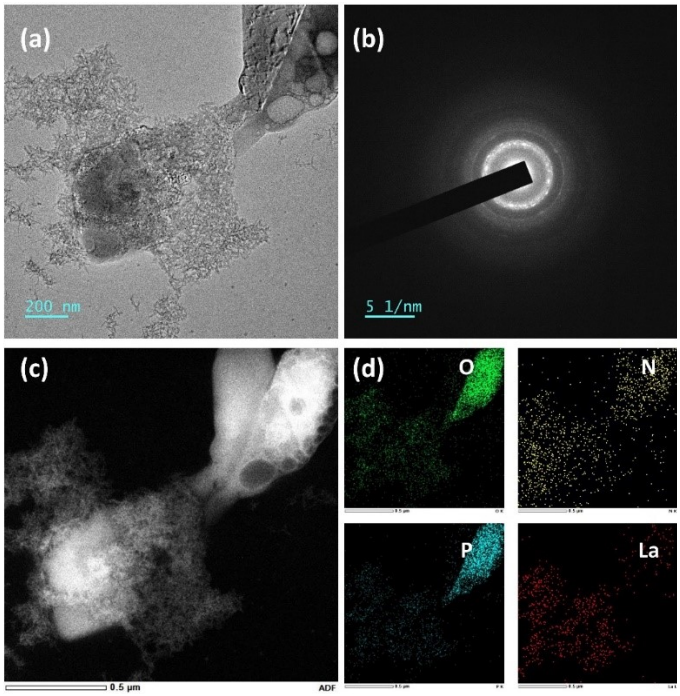

Fig. S9 TEM (a), SAED (b) and EDS-mapping (c-d) images of LaCCH after P saturated.

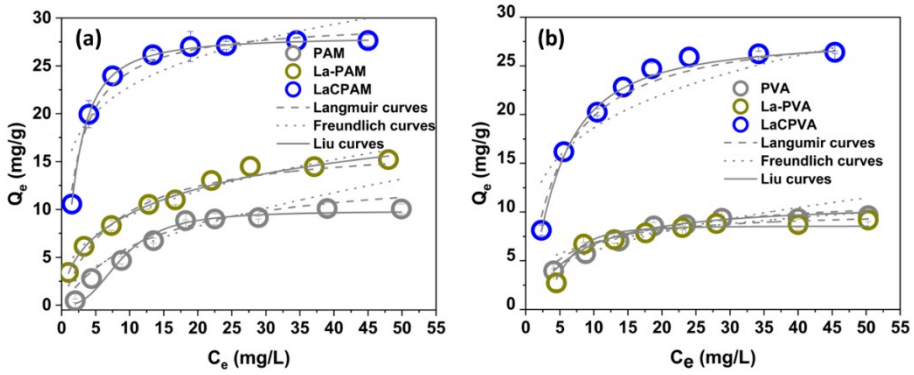

Fig. S10 Adsorption isotherms of PVA/La-PVA/LaCPVA (a) and PAM/La-PAM/LaCPAM (b).

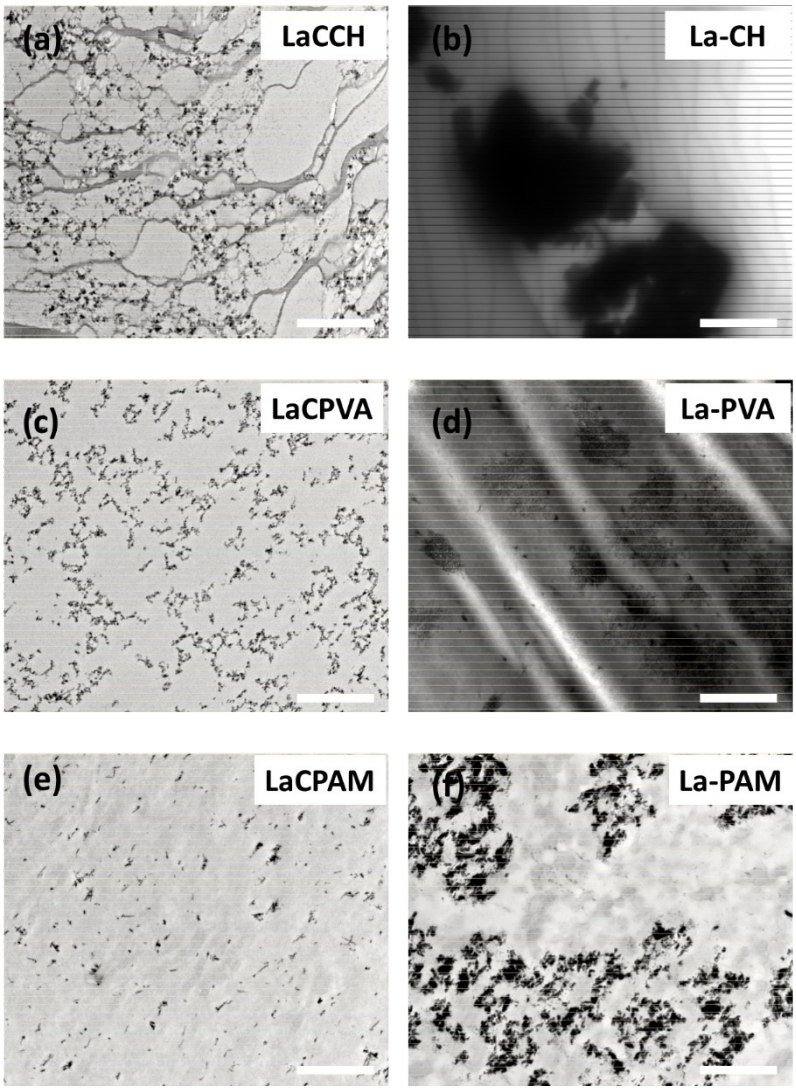

Fig. S11 TEM images of LaCCH (a), La-CH (b), LaCPVA (c), La-PVA (d), LaCPAM (e) and La-PAM (f).

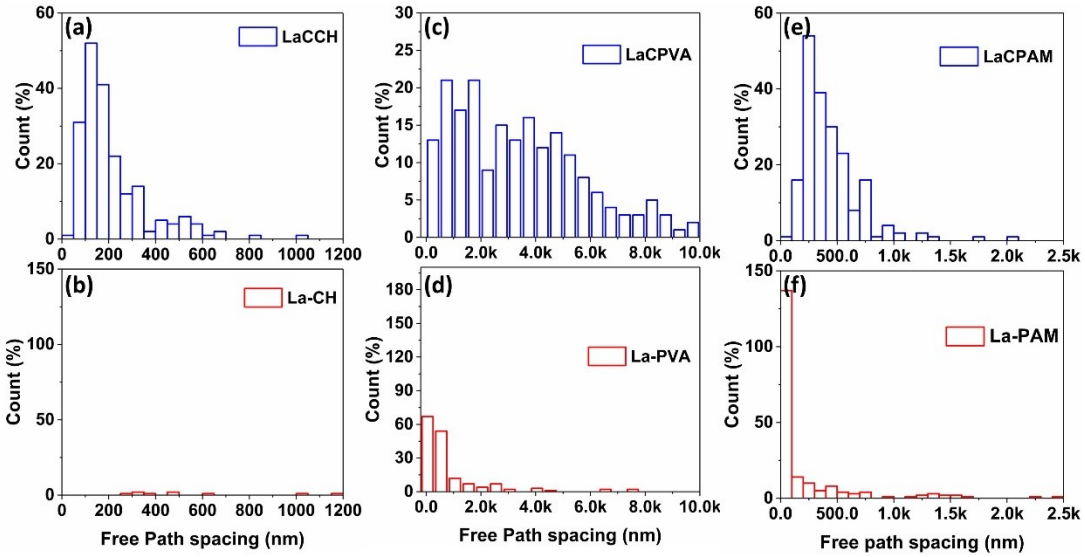

Fig. S12 The distribution of free path spacing corresponding to TEM images: (a) LaCPVA and PVA-La; (b) LaCCH and La-CH; (c) LaCPAM and La-PAM.

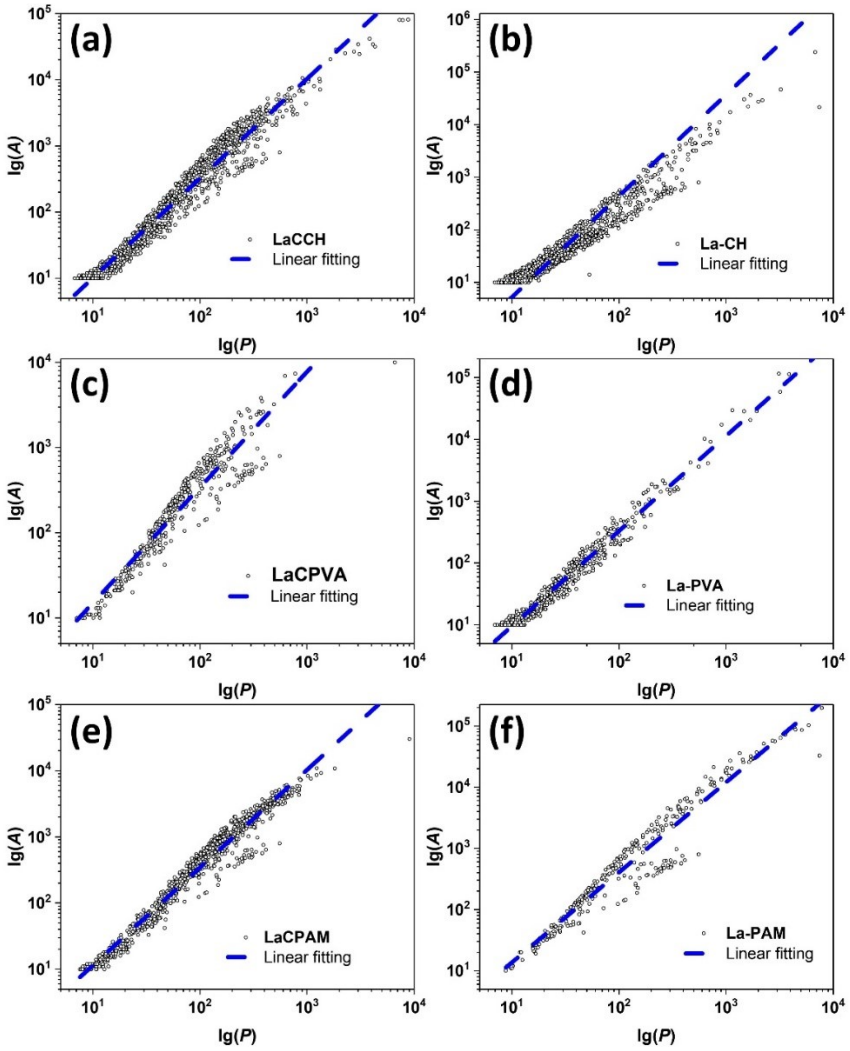

Fig.S13 Dependence of lg perimeter P on lg area A obtained from the binary TEM

images **(Fig. S11)** of La-PVA (a), LaCPVA (b), La-CH (c), LaCCH (d), La-PAM (e) and LaCPAM (f).

Table S1 Parameters of isotherms fitting of LaCCH, La-CH and CH.

Equations	**Langmuir** $q_e = \frac{k_L q_e c}{1 + k_L c}$			**Freundlich** $q_e = k_F c^{\frac{1}{n}}$			**Liu** $q_e = \frac{Q(kx)^n}{1 + (kx)^n}$			
	q_m	k_L	R_L^2	k_F	$1/n$	R_F^2	Q	k	n	R_l^2
LaCCH	108.27	0.124	0.92	16.14	1.82	0.87	75.28	0.25	1.74	0.96
La-CH	87.74	0.09	0.91	10.42	1.72	0.88	57.59	0.20	1.77	0.93
CH	49.08	0.12	0.96	8.10	2.00	0.91	65.64	0.21	1.71	0.98

Table S2 Comparison of phosphorus adsorption capacity for different dephosphorization adsorbents

Adsorbent	pH	Initial concentration (mg/L)	q_m (mg/g)	Ref.
La-MOFs	2.0-11.0	-	87.48-51.50	4
OA-$La(OH)_3$	3.0-11.0	1-100	168	5
LaAl-BTC	2.0-12.0	5–1000	72.27-39.71	6
La@Fe	1.0-13.0	5-600	130–160	7
SCBC-La	3.0-9.0	50-120	48	8
LCM	2.0-10.0	10-100	77.49	9
HKL-LaOH	4.0-10.0	1-200	26.15	10
CCH@La	3.0-9.0	1-50	92.54	11
LDHs-Modified Biochar	3.0-11.0	10-60	10.64	12
FeCa-LDH	4.0-10.0	50-600	-	13
UiO-66-NH_2@$Mg(OH)_2$	4.0-11.0	10-150	130.39	14
FMBO-S	3.0-10.0	5-120	61.24	15
MOF-76(Ce)	3.0-11.0	5-25	72.97	16
Ca_xLa_1-$x$$MnO_3$	3.0-11.0	1-10	37.8	17
$CaFe_{1:2}$-700	3.0-11.0	25-300	62–75	18
MgBC600	3.0-11.0	0.5-160	109.35	19
MMBC-200/600	3.0-11.0	75	83.06	20
Ce-BC	3.0-11.0	1-50	16.7	21

OH/NH_2@MBC	5.0-9.0	-	52.53	22
La-MBC	4.0-8.0	0.5-15	27.49	23
OV-MgO	3.0-11.0	50-100	379.7	24
EFG	4.0-10.0	0-100	49.92	25
LC@AER	6.0-10.0	-	49.89	26
FeCaMg-ALE	2.0-12.0	0-100	20.1	27
Fe/Mn-BMBCs	3.0-11.0	5-150	44.0–53.8	28
Fe^{2+}+HFO	2.0-10.0	5-200	51.7	29
La@PAN	3.0-6.0	10-500	83.33	30
MC-hal-2	3.0-11.0	-	136.7	31
Mg-La LDH	3.0-11.0	100-500	87.23	32
CSPGs-La	2.0-10.0	50-350	159.5	33
La-loaded geopolymer	4.0-12.0	5-60	33.65	34
biochar	2.0-10.0	0-400	98.5	35
LDH-biochar	7.0	0-200	160.8	36
CeAC-A	3.0-11.0	5-120	95.47	37
$Mg_{60}Al_{40}$-LDH	-	1-50	108.8	38
LZ	3.0-10.0	10-150	122.7	39
MGPA DN hydrogel	3.0-12.0	10-150	38.75	40
ZIF-L@GO	3.0-10.0	1-200	116.3 ± 2.1	41
MBC	3.0-11.0	25-200	70.26	42
NH_2-CNS-La	2.0-12.0	5-100	103.01	43
Fe-CLCAB	1.0-9.0	10-200	73.13	44
Ca/(Al-DWTAS)-LDO	2.0-11.0	10-100	110.14	45
CaMgAl-LDH	3.0-11.0	0-150	21.47	46
nano-CaO_2/BFS	4.0-10.0	5-20	67.48	47
MAC@Zr	3.0-9.0	0-50	14.3	48
LaCCH	3.0-11.0	1-50	70.0	This study

Table S3 Kinetics constants for phosphate adsorption on the LaCCH.

Kinetic model		q_e (mg/g)	k_l	R^2
like-pseudo-first-order	$q_t = q_e\left(1 - e^{-k_1 t}\right)$	68.4	9.30	0.950
like-pseudo-second-order	$q_t = \frac{q_e^2 k_2 t}{1 + q_e k_2 t}$	71.37	0.21	0.992

Table S4 Deconvolution of XPS P 2p spectra for LaCCH after P adsorption.

Samples	Species	B.E.[a] (eV)	FWHM[b] (eV)	G:L[c] ratio	Percent[d] (%)
LaCCH	La-PO_4^{3-}	133.1	1.16	0:100	28.8
	La-HPO_4^{2-}	132.1	1.27	14:86	71.2

[a]Binding energy (B.E.); [b]The full width at half maximum (FWHM); [c]Gaussian: Lorentzian ratio; [d]The percentage represents the contribution of each peak to the total number of counts under the P 2p peak.

Table S5 Deconvolution of XPS La 3d spectra for LaCCH sample before and after P adsorption.

Samples	Peak		B.E.[a] (eV)	FWHM [b] (eV)	G:L[c] ratio	Percent[d] (%)
LaCCH	La $3d_{5/2}$	main	835.2	2.63	0:100	31.5
		satellite	839.0	2.4	0:100	29.2
	La $3d_{3/2}$	main	851.9	2.57	2:98	21.8
		satellite	855.8	2.3	0:100	17.6
LaCCH+P	La $3d_{5/2}$	main	835.5	2.1	0:100	23.3
		satellite	837.8	2.9	93:7	40.1
	La $3d_{3/2}$	main	851.1	1.4	0:100	11.2
		satellite	854.3	4.5	9:91	25.1

[a]Binding energy (B.E.); [b]The full width at half maximum (FWHM); [c]Gaussian: Lorentzian ratio; [d]The percentage represents the contribution of each peak to the total number of counts under the P 2p peak.

Table S6 Deconvolution of XPS O 1s spectra for LaCCH sample before and after P adsorption.

Samples	Species	B.E.[a] (eV)	FWHM[b] (eV)	G:L[c] ratio	Percent[d] (%)
LaCCH	La–O	531.7	2.6	0:100	85.0
	-OH	529.5	1.1	0:100	15.0
LaCCH +P	La–O	532.0	1.8	0:100	27.9

	-OH	530.5	1.5	18:82	45.4
		531.6	1.1	19:81	26.7

[a]Binding energy (B.E.); [b]The full width at half maximum (FWHM); [c]Gaussian: Lorentzian ratio; [d]The percentage represents the contribution of each peak to the total number of counts under the P 2p peak.

References:

1. I. Langmuir, The adsorption of gases on plane surfaces of glass, mica and platinum, *J. Am. Chem. Soc.*, 1918, **40**, 1361-1403.
2. A. Mittal, L. Kurup and J. Mittal, Freundlich and Langmuir adsorption isotherms and kinetics for the removal of Tartrazine from aqueous solutions using hen feathers, *Journal of Hazardous Materials*, 2007, **146**, 243-248.
3. H. N. Tran, E. C. Lima, R.-S. Juang, J.-C. Bollinger and H.-P. Chao, Thermodynamic parameters of liquid–phase adsorption process calculated from different equilibrium constants related to adsorption isotherms: A comparison study, *J. Environ. Chem. Eng.*, 2021, **9**, 106674.
4. Q. He, H. Zhao, Z. Teng, Y. Guo, X. Ji, W. Hu and M. Li, Tuning microscopic structure of La-MOFs via ligand engineering effect towards enhancing phosphate adsorption, *Journal of Environmental Management*, 2024, **353**, 120149.
5. L. Hu, G. Zhan, L. Zhao, J. Dai, X. Zou, J. Wang, W. Hou, H. Li, Y. Yao and L. Zhang, Monodispersed and Organic Amine Modified La (OH) 3 Nanocrystals for Superior Advanced Phosphate Removal, *Advanced Materials*, 2024, 2400870.
6. Z. Zhu, L. Qin, Y. Liu, Q. Zhang, P. Cheng and W. Liang, Fabrication and mechanism of La/Al bimetallic organic frameworks for phosphate removal, *Chemical Engineering Journal*, 2024, **479**, 147081.
7. G. Li, Y. Zhang, X. Hu, T. Wei, J. Li, W. Hongbin and X. Wang, A study on the performance of a recyclable adsorbent La@ Fe for phosphate adsorption in wastewater, *Process Safety and Environmental Protection*, 2024, **188**, 25-38.
8. E. Zong, Y. Shen, J. Yang, X. Liu and P. Song, Preparation and characterization of an invasive plant-derived biochar-supported nano-sized lanthanum composite and its application in phosphate capture from aqueous media, *ACS omega*, 2023, **8**, 14177-14189.
9. B. Liu, J. Nan, R. Jiang, F. Wu, L. Song, Z. Ge, X. Ye, X. Zhang and W. Wang, Three-dimensional porous aerogel-bead absorbent with high dispersibility of lanthanum active sites to boost phosphorus scavenging, *Chemical Engineering Journal*, 2023, **451**, 138509.
10. S. Zheng, J. Fan and X. Lu, Heated kaolinite-La (III) hydroxide complex for effective removal of phosphate from eutrophic water, *Applied Clay Science*, 2023, **231**, 106729.
11. X. Li, Y. Wang, S. Dong, C. Liu, S. Wang and W. Liu, Tuning the lanthanum hydrolysis induced assembly process using long linear chains with–N+ (CH3) 3 groups for efficient phosphate removal, *Chemical Engineering Journal*, 2023, **451**, 138713.
12. C. Ding, X. Long, G. Zeng, Y. Ouyang, B. Lei, R. Zeng, J. Wang and Z. Zhou, Efficiency recycling and utilization of phosphate from wastewater using LDHs-modified biochar, *International Journal of Environmental Research and Public Health*, 2023, **20**, 3051.

13. W. Feng, H. Cui, H. Zhu, B. Shutes, B. Yan and S. Hou, Layered double hydroxides, an effective nanomaterial to remove phosphorus from wastewater: performance, mechanism, factors and reusability, *Science of The Total Environment*, 2023, **884**, 163757.
14. Y. Yan, Y. Zhao, C. Gong, Y. Tao, K. Lu, X. Hong, M. Xia and F. Wang, In-situ growth of 2D magnesium hydroxide on zirconium-based metal organic frameworks for phosphate removal: an experimental and theoretical exploration of adsorption behavior, *Separation and Purification Technology*, 2023, **304**, 122289.
15. J. Yun, N. K. Shahi and S. Dockko, Adsorption performance and mechanism of a starch-stabilized ferromanganese binary oxide for the removal of phosphate, *Chemosphere*, 2024, **362**, 142864.
16. F. Civan Çavuşoğlu, G. Ozcelik and S. S. Bayazit, Comparative Investigation of Phosphate Adsorption Efficiencies of MOF-76 (Ce) and Metal Oxides Derived from MOF-76 (Ce), *Langmuir*, 2024, **40**, 4255-4266.
17. M. Feng, M. Li, C. Guo, M. Yuan, L. Zhang, S. Qiu, W. Fu, K. Zhang, H. Guo and F. Wang, Green synthesis of CaxLa1-xMnO3 with modulation of mesoporous and vacancies for efficient low concentration phosphate adsorption, *Journal of Environmental Management*, 2024, **351**, 119837.
18. M. H. P. Araújo, J. D. Ardisson, A. C. Krohling, R. M. Lago, W. G. Júnior and J. C. Tristão, Calcium ferrites for phosphate adsorption and recovery from wastewater, *RSC advances*, 2024, **14**, 1612-1624.
19. C.-Y. Wang, H.-D. Zhou, Q. Wang, B.-X. Xu and G. Zhu, Efficiency and mechanism of phosphate adsorption and desorption of a novel Mg-loaded biochar material, *Environmental Science and Pollution Research*, 2024, **31**, 4425-4438.
20. Y. Yin, Y. Xu, Z. Zhao, Y.-n. Luan, Y. Xiao and C. Liu, Nanoscale MgO confined in magnetic biochar via two-step pyrolysis for enhanced phosphate adsorption, *Separation and Purification Technology*, 2024, **339**, 126754.
21. Y. Yue, Z. Zeng, Y. Zhou and W. Hu, Phosphate adsorption characteristics of CeO2-loaded, Eucommia ulmoides leaf residue biochar, *Environmental Pollution*, 2024, **360**, 124657.
22. X. Zhang, Y. Xiong, X. Wang, Z. Wen, X. Xu, J. Cui, Z. Liu, L. Wei and X. An, MgO-modified biochar by modifying hydroxyl and amino groups for selective phosphate removal: Insight into phosphate selectivity adsorption mechanism through experimental and theoretical, *Science of The Total Environment*, 2024, **918**, 170571.
23. Y. Yi, Y. Fu, Y. Wang, Z. Xu and Z. Diao, Lanthanum/iron co-modified biochar for highly efficient adsorption of low-concentration phosphate from aqueous solution, *Journal of Environmental Chemical Engineering*, 2024, **12**, 111876.
24. Q. Hu, S. Pang, Y. Li, L. Huang, Y. Zhang, X. Xu and X. Pei, Enhanced removal of phosphate from aqueous solutions by oxygen vacancy-rich MgO microspheres: Performance and mechanism, *Chemosphere*, 2024, **355**, 141776.
25. C. Sun, C. Huang, P. Wang, J. Yin, H. Tian, Z. Liu, H. Xu, J. Zhu, X. Hu and Z. Liu, Low-cost eggshell-fly ash adsorbent for phosphate recovery: A potential slow-release phosphate fertilizer, *Water Research*, 2024, **255**, 121483.
26. Y. Zhang, Z. Zheng, M. A. Badsha and I. M. Lo, Advancing phosphate Removal: Unleashing the Adsorption/Desorption potential of La2 (CO3) 3-Loaded resin by Semi-Fluidized columns and In-Situ regeneration, *Separation and Purification Technology*, 2024, **341**, 126835.

27. Q. Kong, P. Wang, B. Song, Y. Lan, W. Ma, X. Shi, L. Xiao, G. Zhu, P. Wang and J. Lian, Sludge-derived alginate-like extracellular polymers (ALE) for preparation of Fe-ALE and FeCaMg-ALE: Application to the adsorption of phosphate, *International Journal of Biological Macromolecules*, 2024, **279**, 134995.
28. N. Che, J. Qu, J. Wang, N. Liu, C. Li and Y. Liu, Adsorption of phosphate onto agricultural waste biochars with ferrite/manganese modified-ball-milled treatment and its reuse in saline soil, *Science of The Total Environment*, 2024, **915**, 169841.
29. X. Wang, Y. Li, X. Wen, L. Liu, L. Zhang and M. Long, Cooperation of ferrous ions and hydrated ferric oxide for advanced phosphate removal over a wide pH range: Mechanism and kinetics, *Water Research*, 2024, **249**, 120969.
30. Y. Zhang, R. Xi, S. Du, L. He, Z. Li, M. Yang, K. Zhu, W. Xu and D. Song, Lanthanum-loaded polyacrylonitrile fiber as an efficient phosphate adsorbent, *Separation and Purification Technology*, 2024, 129416.
31. D. Jiang, X. Long, M. Xiang, X. Gan, Q. Pu, Y. Chen, N. Qi and X. Wang, Evaluation of magnetic calcium silicate hydrate derived from halloysite clay for efficient phosphate capture, *Journal of Environmental Chemical Engineering*, 2024, **12**, 112233.
32. Y. Xu, Y. Yin, Y.-N. Luan, Q. Wang, Z. Zhao, Z. Guo and C. Liu, Efficient phosphate removal by Mg-La binary layered double hydroxides: synthesis optimization, adsorption performance, and inner mechanism, *Environmental Science and Pollution Research*, 2024, **31**, 29132-29147.
33. J. Wu, Y. Zhong, C. Hao, J. Chen, H. Gao, S. Han, Y. Shen and X. Wang, Emulsion synthesis of cellulose/lanthanum alginate/La (Ⅲ) composite microspheres for efficient and selective adsorption of phosphate, *Chemical Engineering Journal*, 2024, **488**, 150949.
34. G. J. Savoir and T. Wu, Lanthanum-loaded geopolymer for phosphate removal from agricultural runoff, *Science of The Total Environment*, 2024, **948**, 174390.
35. Y. Manawi, R. Al-Gaashani, S. Simson, Y. Tong, J. Lawler and V. Kochkodan, Adsorptive removal of phosphate from water with biochar from acacia tree modified with iron and magnesium oxides, *Scientific Reports*, 2024, **14**, 17414.
36. W.-H. Huang, Y.-J. Chang and D.-J. Lee, Layered double hydroxide loaded pinecone biochar as adsorbent for heavy metals and phosphate ion removal from water, *Bioresource Technology*, 2024, **391**, 129984.
37. T. Zhang, S. Shan, D. Liu, Y. Han, K. Sun and W. Wang, Cerium-based sorbent with 100% Ce (III) and high dispersion for enhanced phosphate removal from wastewater, *Chemical Engineering Journal*, 2024, **497**, 154385.
38. Q. Tong, P. Cheng, G. Jiang, Y. Li, Y. Wei, Y. Zou, X. Lv and L. Ao, Hierarchical flower-like MgAl layered double hydroxide microparticles as phosphate porter for its recovery from phosphate-contaminated water, *Separation and Purification Technology*, 2024, **330**, 125384.
39. Q. Luo, J. Wei, Z. Guo and Y. Song, Adsorption and immobilization of phosphorus from water and sediments using a lanthanum-modified natural zeolite: Performance, mechanism and effect, *Separation and Purification Technology*, 2024, **329**, 125187.
40. W. Zhang, Y. Wu, H. Chen, Y. Gao, L. Zhou, J. Wan, Y. Li, M. Tang, Y. Peng and B. Wang, Efficient phosphate removal from water by multi-engineered PVA/SA matrix double network hydrogels: Influencing factors and removal mechanism, *Separation and Purification Technology*, 2024, **336**, 126261.
41. X. Zou, H. Zhang, L. Xiang, C. Huang and J. Li, Designing a dual-functional ultrathin ZIF-L@

GO adsorbent for simultaneous removal of phosphate and tetracycline hydrochloride: Adsorption capacity and mechanism, *Colloids and Surfaces A: Physicochemical and Engineering Aspects*, 2024, **683**, 132851.

42. Y. Liu, S. Wang, J. Huo, X. Zhang, H. Wen, D. Zhang, Y. Zhao, D. Kang, W. Guo and H. H. Ngo, Adsorption recovery of phosphorus in contaminated water by calcium modified biochar derived from spent coffee grounds, *Science of the Total Environment*, 2024, **909**, 168426.
43. J. Li, Y. Huang, Z. Pan, J. Ni, W. Yang, Y. Zhang, Y. Zhang and Y. Li, One-pot fabrication of functional groups-rich carbonaceous nanosheets with TEDA assisted anchoring well-dispersed La (OH) 3 for enhanced phosphate removal, *Separation and Purification Technology*, 2024, **330**, 125355.
44. A. Manna, S. Lahiri, K. Sen and K. Banerjee, Fe (III) cross-linked cellulose-agar hydrogel beads for efficient phosphate removal from aqueous solutions, *Environmental Monitoring and Assessment*, 2024, **196**, 54.
45. N. Xie, L. Yi, J. Li, W. Wang, T. Gu, M.-G. Ma, S. Wang and S. Liu, A green synthesis strategy toward calcined calcium-aluminum layered double hydroxide with sludge as aluminum source for efficient removal of phosphate from water, *Surfaces and Interfaces*, 2024, **46**, 104075.
46. V. Jurado-Davila, I. A. H. Schneider and L. A. Féris, Synthesis of Ca-Mg-Al layered double hydroxide from dolomite with ultrasound-assisted method. Application in phosphate removal, *Inorganic Chemistry Communications*, 2024, **159**, 111829.
47. S. Shan, L. Wu, S. Qu, D. Li and Y. Huang, Efficient removal and recovery of phosphate from wastewater by nano-CaO2/BFS sorbent and its potential as a slow-release phosphate fertilizer, *Water-Energy Nexus*, 2024, **7**, 163-174.
48. Y. Zhang, P. Chen, J. Luo, X. Yang and L. Fan, Selective and efficient capture of phosphate from aqueous solution using magnetic zirconium-loaded coconut shell carbon materials: Kinetic and mechanism study, *Journal of Water Process Engineering*, 2024, **66**, 106069.